



Quantifying the impact of a smart farming system application on local-scale air quality of smallhold farms in Greece

Evangelia Fragkou¹ · George Tsegas¹ · Athanasios Karagkounis¹ · Fotios Barmpas¹ · Nicolas Moussiopoulos¹

Received: 17 January 2022 / Accepted: 21 September 2022 / Published online: 10 October 2022
© The Author(s) 2022

Abstract

Smart farming (SF) has emerged as a scientific approach exploiting technology advances for the management of agricultural practices, focusing on the control of resources and chemicals used. There is still limited evidence in the scientific literature in regard to the efficiency of SF, particularly for targeted environmental issues, such as air pollutant emissions from agricultural activities. The present paper exploits quantitative data collected from questionnaires to farmers of 6 pilot areas in Greece, participating in the LIFE GAIA Sense project. Emissions and pollutant levels were calculated for two consecutive years in these pilot areas, namely 2019 (baseline year) and 2020, which is the first SF application year. The methodology for calculating realistic emissions data, following a combined tier 1/tier2 approach is presented. To this purpose, detailed activity data of the specific SF application areas related to agricultural activities were acquired, based on the responses of participating farmers to targeted questionnaires. Calculated emissions were used as input data for air quality modeling simulations to examine the efficiency of SF in reducing local pollutant concentrations. The results show significant emissions and concentrations reductions in five out of the six pilot areas, for all pollutants and greenhouse gases studied, due to the decrease in fuel consumption and N fertilizer applied, as a result of the farmers following the SF advice. Particularly for NH₃, which is an agricultural air pollutant of concern due to its health and environmental impacts, emission reductions of around 30% (and by up to almost 60%) were calculated.

Keywords Agricultural air pollutant and greenhouse gas emissions · Air pollution modeling · Air pollution management · Smart farming · Sustainable agriculture

Introduction

An important environmental pressure of agricultural activities relates to air quality deterioration. Agriculture is a common driver for both air pollution and climate change and these feedback mechanisms have to be considered when assessing the relevant environmental impacts of agricultural practices. Many agricultural activities rely on energy consumption of relevant machinery and equipment, resulting to significant emissions of greenhouse gases (GHGs) and air pollutants, including carbon dioxide, nitrogen oxides, and particulate matter (mainly PM_{2.5} and PM₁₀). Activities throughout the life cycle of agricultural products and

livestock that rely on fossil fuel usage, e.g., energy required for heating/lighting and cooling in greenhouses and livestock premises, for routine agricultural activities (ploughing, spraying, harvesting, shredding, etc.), and for the transport/loading of the products to shelves of retailers are important emitters. All the above agricultural activities also emit a significant amount of particulate matter, accounting for around 16% of PM₁₀ emissions in the EU emission inventory of 2019 (EEA 2019a). Furthermore, N₂O emission from croplands as a result of biological nitrification and denitrification processes in soils is an important contributor in GHGs emissions in Europe. According to the latest EU GHG inventory, GHG emissions in the agricultural sector represent almost 10% of the total EU GHG emissions (EEA 2019b). Fertilizer application in agricultural soils is an important agricultural source of ammonia (NH₃), nitrogen oxides (NO_x), and nitrous oxide (N₂O) emissions, accounting for 93%, 8% (EEA 2019a), and 5.9% (EEA 2019b) of total EU emissions, respectively. In particular, the alkaline ammonia emissions

✉ Evangelia Fragkou
evfragkou@auth.gr

¹ Laboratory of Heat Transfer and Environmental Engineering, Department of Mechanical Engineering, Aristotle University of Thessaloniki, Thessaloniki, Greece

from N fertilizer application contribute to the formation of inorganic fine airborne particulate matter ($PM_{2.5}$), following the reaction with sulfuric and nitric acid (Erisman and Schaap 2004), with significant health and climatic effects.

To reduce farming-related atmospheric emissions, appropriate technology tools and methodologies to realistically evaluate atmospheric impacts and suggest mitigation options at farm level may be of use to farmers and policy makers. In this frame, the European Commission funds research and demonstration projects aiming to develop data-driven Decision Support Systems to promote sustainable agricultural practices, taking advantage of state-of-the-art technological advances covered by the umbrella term “Smart Farming” (SF). SF refers to the exploitation of real-time data relevant to agricultural activities by farmers in order to optimize their use of chemicals (fertilizers, pesticides) and natural resources (water, energy), so as to reduce the associated cost and environmental impact, while retaining or, ideally, increasing crop yield. SF applications represent an emerging and promising digital agriculture methodology, as relevant data are collected via remote sensing and monitoring sensors of low-cost (e.g., for measuring air quality, meteorological parameters), and are then distributed to farmers via smart systems such as the Internet of Things (IoT) platforms, Big Data, artificial intelligence, and cloud computing (Lieder and Schröter-Schlaack 2021).

An example of a European developed SF system is demonstrated in the GAIA Sense Smart Farming application, which has been developed as a resource efficiency tool for agricultural enterprises. The project LIFE GAIA Sense (URL 1) targets agriculture related environmental issues through the development and application of an innovative SF system that aims at reducing the consumption of natural resources and minimizing environmental impact, while increasing crop production. Its main purpose is to monitor crops, collect high-resolution environmental data, and offer advice about irrigation, fertilization and pesticides based on site-specific soil, weather, and plant nutrition data. This philosophy leads to an increase of resource efficiency, promoting sustainable and circular economy in the agriculture sector. One of the main objectives of the project is to evaluate and quantify the environmental impact of the GAIA Sense application in terms of air, soil and water pollution by implementing 18 demonstration pilot campaigns across Greece, Spain, and Portugal.

SF applications are not strongly supported by current policy regulation, according to the workshop report of the European Commission’s Joint Research Centre, which took place in the Milan World Expo, with the theme “Feeding the planet, energy for life,” in 2015. This lack of policy action reflects lack in awareness among public and sector stakeholders, partly stemming from inadequate scientific evidence and quantified results. A number of scientific efforts have

focused on a review of opportunities and risks related to SF (Lieder and Schröter-Schlaack 2021), but quantification of individual environmental gains at farm level is still lacking. In terms of air quality improvement, estimation of agricultural emissions of air pollutants is primarily directed toward national or state scales (Almaraz et al. 2018; Gu et al. 2018), while research and statistical analysis of results on a farm-level are very scarce. As emissions of air pollutants from agricultural activities affect primarily exposure of farmers and farm workers, as well as populations of surrounding areas, it is important to assess the improvement of local air quality as a result of SF application. By collecting, synthesizing, and statistical analysis of farm level air pollutant emissions and concentration data from many small farms, it will be possible to draw scientifically based conclusions on the efficiency of SF on a larger, e.g., national, scale (bottom-up technique).

The scientific evidence necessary for evaluating the efficiency of the SF system application in terms of air quality improvement requires an integrated approach, including preparation of a process-based emissions inventory for the specific geographical area of the pilot farm and time period at an appropriate resolution, and based on these farm-specific emissions data, the quantification of any reductions in pollutant concentrations. Although measured data from on-site sensors are of indisputable value for characterizing farm-scale air quality, monitoring stations cannot cover all regions and periods of interest to study spatial and temporal variability of air pollutants over an agricultural area. For this purpose, air quality models are the only scientifically relevant tools. Pollutant dispersion models describe the physical and chemical processes in the atmosphere which control the transport and transformation of emitted air pollutants and are thus able to realistically simulate their spatial and temporal distribution. Air pollution modeling related to agricultural atmospheric emissions during the last decade has mainly been limited to ammonia dispersion simulations, as ammonia dispersion characteristics were not satisfactorily represented in initial agricultural air quality simulations (Zhang et al. 2008). Different dispersion models (e.g., the advanced Gaussian Atmospheric Dispersion Modeling System AERMOD and the AMS/EPA Regulatory Model ADMS) have been compared in terms of their ability to accurately simulate ammonia concentration dispersion patterns, focusing on individual processes, such as dry deposition (Theobald et al. 2012). Significant research efforts document the development and implementation of dynamical ammonia emission parameterization in air pollution models, particularly accounting for temporal variability (Gyldenkerne et al. 2005). Finally, for air quality management purposes, a number of papers have employed air pollution simulations to estimate the impact of agricultural ammonia emissions reduction on air quality,

particularly in terms of particulate matter formation (Zhao et al. 2017; Pozzer et al. 2017). An important aspect affecting model accuracy is the spatial representativity, as spatial variability of emissions and subgrid variations of concentrations is a significant source of uncertainty in model results (Park et al. 2006).

In view of the above issues, the present paper aims to enhance scientific evidence and provide demonstrable benefits in regard to the efficiency of SF in reducing agriculture related environmental impacts, by presenting an integrated methodology and statistical results for quantifying the benefits on air quality at farm-scale resulting from the GAIA Sense system application in smallholder farms in Greece. The first step of the methodology involves calculating the emissions of atmospheric pollutants and GHGs emitted from the agricultural activities in six GAIA Sense pilot areas in Greece, representing five different crop types. The Lagrangian air pollutant dispersion model AUSTAL is then deployed for assessing the impact of agricultural activities on the local air pollution levels.

Methodology for evaluation of the SF system

The methodology followed to assess the impact of application of the SF advice in each pilot area in terms of local air quality is described in detail in the following paragraphs. The SF advice in the GAIA Sense system is adapted to the requirements of each crop field, as it is based on day-by-day analysis of historical data on meteorology, soil variables, and farming activities performed and on forecasting of relevant meteorological and soil parameters data for the specified region. In particular, the fertilization models used are calibrated for each pilot area, using (a) geospatial and geographical data for the particular field location, (b) crop information, such as crop variety and plant age, as well as (c)

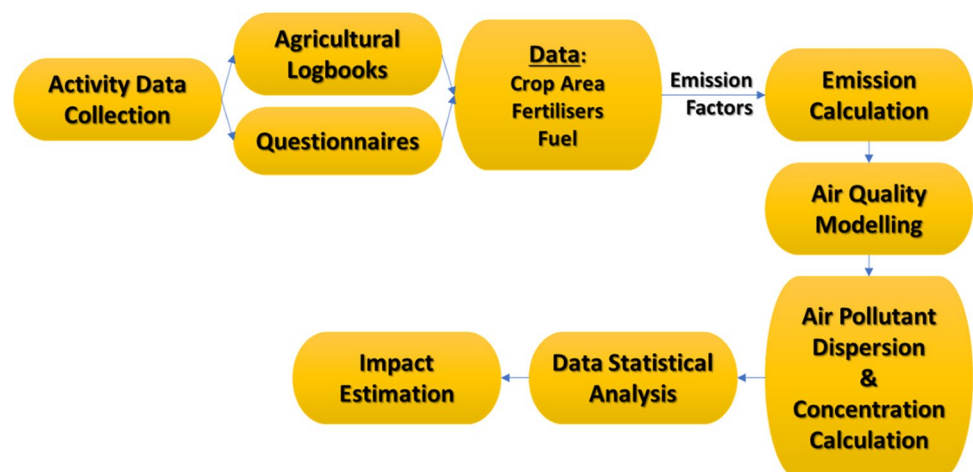
information from soil samples regarding soil type/composition, pH, nutrient content, and (d) information from gaitron telemetric sensors in respect to meteorological parameters, including wind speed and direction, temperature, soil moisture, rainfall, and radiation. The data are analyzed and integrated into the fertilization models which are then used to synthesize the collected data and provide recommendations to farmers on proper fertilization quantity and chemical context, according to the specific requirements of each location and crop type. This advice is presented to farmers via the dedicated applications of the system, which are either web-based or mobile applications.

The steps followed in the methodology of the present study (Fig. 1) involved the processes of (1) raw data collection and analysis, (2) extraction of emissions factors (EFs) from official national guidebooks, (3) calculation of emissions of all legislated atmospheric pollutants, (4) retrieval and preparation of other input data (including meteorology and geographical data) for dispersion modeling simulations, (5) calculation of pollutant concentrations and dispersion patterns, and, as a final step (6) statistical analysis of results between the two studied years for the integrated evaluation of the efficiency of the GAIA Sense SF system, in terms of local air quality improvement. The methodological steps are described in detail in the following sections.

Methodology for emissions calculation

Realistic emission data are a pre-requisite for reliable modeling estimation of the impact of agricultural activities on local air quality. Availability of high temporal and spatial resolution of pollutant emissions in smart farming applications is of particular importance in order to assess the local impact on the atmospheric environment. Atmospheric pollutant emissions are calculated by multiplying the activity rate with an emission factor. In the suggested methodology presented in this paper, emission factors from the EMEP/

Fig. 1 Methodological steps for the integrated evaluation of the GAIA Sense SF system in respect to local air quality improvement



EEA air pollutant emission inventory guidebook 2019 (EMEP/EEA 2019a, b) and particularly of the 1A (mobile machinery) and 3D (crop production and agricultural soils) NFR categories were used for most of the studied pollutants. For calculation of N_2O emissions resulting from fertilization of agricultural soil, the IPCC reference emission factor of 1% of kg N fertilizer applied is used. The proposed modeling methodology relies on the calculation of realistic emissions data following a combined tier 1 and tier 2 approach for emission calculation. For this purpose, detailed activity data of the specific SF application pilot areas related to agricultural activities were acquired.

Activity data for the specific smart farming applications were based on the compilation and analysis of the responses of participating farmers to targeted questionnaires. The questionnaires were structured including three categories of questions in relation to social, economical, and environmental indicators in order to obtain the necessary quantitative information for an integrated impact assessment of the SF system in the participating pilot agricultural parcels. A set of environmental indicators specifically targeted the impact on the atmospheric environment and were included to provide quantitative activity data for calculating the related atmospheric pollutant emissions. These indicators particularly included the use of fertilizers and energy use. The related questions required specifically the following information:

1. Use of chemical and organic fertilizers—type (composition) and quantity (annual quantity in kg per ha) of fertilizer for the specific crop type and the application frequency (e.g., per year or season)

2. Energy use—annual consumption of transport fuel in liters

The quantitative replies of the farmers in the aforementioned questions were combined with the information they entered in their agricultural logbooks and with specific information regarding soil properties (pH in particular) from GAIA Sense monitoring IoT devices, called GAIAtrons. GAIAtrons are telemetric autonomous stations that collect data from sensors installed in the field and record atmospheric and soil parameters in the GAIA Sense pilot farm areas.

In regard to the available sample size, 17 farmers from 6 different pilot regions across Greece, which are representing a range of five crop types, provided usable data. Figure 2 demonstrates the geographical region of each pilot area and the corresponding crop type.

Regarding collection of raw data, a number of 17 completed questionnaires were received, out of which seven reported quantitative information on both fertilizers used and fuel consumption, while the rest of them (10/17), provided data only on fertilizer application. In order to increase data accuracy for the statistical analysis of the study, fertilizer data from questionnaires were compared and completed with available relevant data from agricultural logbooks for the majority of the participating fields (12/17). Agricultural croplogs are completed with quantitative data in real-time, namely shortly after the specific agricultural activity has taken place and are thus considered more realistic compared to data reported by farmers in the questionnaires, which are

Fig. 2 Map of the six studied pilot areas in Greece representing five different crop types



completed as mean quantities at the end of the cultivating year.

Two consecutive years were compared for evaluating the SF system efficiency, 2019 (baseline cultivation period) and 2020 (SF application year). Table 1 presents changes in the total amount of nitrogen (N) from fertilizers applied, as well as in the fuel consumed for all relevant transportation between the two studied years, in the 17 pilot fields. Absolute values are reported for each year, along with % changes. As a result of conforming to SF advice for agricultural practices, significant reductions are observed in the majority of the fields both for N application (N fertilizer use was reduced in 13 out of the 17 pilot fields, reaching values of -50%), as well as for fuel consumption (reduction in five out of 7 pilot fields, reaching values of -40%). However, in a few pilot fields, significant increases are also noted, such as in the case of a 60.5% increase in fertilizer application in Stylida 5 and in the case of 70% increase in fuel consumption in Mirabello 4. These positive changes can be attributed to the fact that in some cases farmers chose not to follow

the SF advice, or to other reasons, e.g., related to fertilization timing and frequency depending on meteorological conditions for the increase in N fertilizer application, or the use of different transport equipment for the increase in fuel consumption.

In Table 2, data from individual pilot fields are shown averaged over each pilot region, in order to present them in relation to their geographical location. Averaged data for fuel consumption have absorbed the positive change in the case of Mirabello 4, leading to an overall decrease of 19.8% in the Mirabello pilot region, but in respect to fertilizer application, the large increase reported in the pilot field of Stylida 5 (and to a less extent in Stylida 4) resulted in a significant overall positive change of 26.4% in the pilot field area of Stylida for olive crop.

Based on the above on-site activity and soil data acquired from the questionnaires and field monitors (imported in the agricultural logbooks), a methodology to calculate realistic emissions of atmospheric pollutants and GHGs was structured depending on pollutant type, as follows:

Table 1 Absolute values of nitrogen (N) in fertilizers applied and fuel consumed for the two cultivation years and their relative percentage changes in the 17 participating pilot fields

| Pilot field | N in fertilizers (kg/ha) | | | Fuel consumption (lt/ha) | | |
|----------------------|--------------------------|--------|------------|--------------------------|--------|------------|
| | 2019 | 2020 | Change (%) | 2019 | 2020 | Change (%) |
| Elassona 6 (Walnut) | 66.37 | 46.5 | -29.94 | 316.46 | 316.46 | 0 |
| Mirabello 2 (Olive) | 144 | 84 | -41.67 | 222.22 | 133.33 | -40 |
| Mirabello 4 (Olive) | 160 | 104 | -35 | 50 | 85 | 70 |
| Pella 3 (Peach) | 60 | 60 | 0 | 100 | 62.5 | -37.5 |
| Pella 4 (Peach) | 88 | 80 | -9.09 | 88.24 | 73.53 | -16.67 |
| Pella 5 (Peach) | 96 | 90 | -6.25 | 192.31 | 128.21 | -33.33 |
| Stylida 3 (Olive) | 35.18 | 26.08 | -25.87 | - | - | - |
| Stylida 4 (Olive) | 76 | 95 | 25 | 561.8 | 524.3 | -6.67 |
| Stylida 5 (Olive) | 57 | 91.5 | 60.53 | - | - | - |
| Pieria 1 (Kiwi) | 288.66 | 149.39 | -48.25 | - | - | - |
| Pieria 2 (Kiwi) | 303.06 | 154.6 | -48.99 | - | - | - |
| Pieria 3 (Kiwi) | 211.59 | 152.39 | -27.98 | - | - | - |
| Pieria 4 (Kiwi) | 197.76 | 165.19 | -16.47 | - | - | - |
| Pieria 5 (Kiwi) | 232.71 | 210.19 | -9.68 | - | - | - |
| Orestiada 1 (Cotton) | 164 | 85.5 | -47.87 | - | - | - |
| Orestiada 3 (Cotton) | 170.2 | 178 | 4.58 | - | - | - |
| Orestiada 7 (Cotton) | 132 | 66 | -50 | - | - | - |

Table 2 Absolute values of nitrogen (N) in fertilizers applied and fuel consumed for the two cultivation years and their relative percentage changes, averaged over each pilot region

| Pilot Area | N in fertilizers applied (kg/ha) | | | Fuel consumption (lt/ha) | | |
|--------------------|----------------------------------|-------|------------|--------------------------|-------|------------|
| | 2019 | 2020 | Change (%) | 2019 | 2020 | Change (%) |
| Elassona (Walnut) | 66.4 | 46.5 | -29.9 | 316.5 | 316.5 | 0 |
| Mirabello (Olive1) | 152 | 94 | -38.2 | 136.1 | 109.2 | -19.8 |
| Pella (Peach) | 81.3 | 76.7 | -5.7 | 126.8 | 88.1 | -30.6 |
| Stylida (Olive2) | 56.1 | 70.9 | 26.4 | 561.8 | 524.3 | -6.67 |
| Pieria (Kiwi) | 246.8 | 166.4 | -32.6 | - | - | - |
| Orestiada (Cotton) | 155.4 | 109.8 | -29.3 | - | - | - |

- Tier 1 methodology was applied to calculate emissions of PM₁₀, PM_{2.5}, NO, and NMVOC, using the default emission factors (EFs) for NFR Source category 3.D (crop production and agricultural soils) from Table 3.1 of the EMEP EMEP/EEA air pollutant emission inventory guidebook 2019 (EMEP/EEA, 2019a, b). This source category includes emissions related to the application of N fertilizers (for NO), emissions from standing cultivated crops (for NMVOC) and farm-level agricultural operations (for particulate matter), such as ploughing, spraying, harvesting, and storage/handling of agricultural product. On-site data for quantities of fertilizer (kg of fertilizer N) applied and size of the cultivated area (ha) were derived from farmers' questionnaires and logbooks. The percentage of N of each fertilizer was estimated from the fertilizer composition.
- Tier 1 methodology was used for emissions calculation of GHGs (CH₄, CO₂, N₂O) and atmospheric pollutants (NH₃, NMVOC, NO_x, PM₁₀, and PM_{2.5}), employing the default EFs for NFR Source category 1.A.4.c.ii-Agriculture from Table 3-1 (Tier 1 emission factors for off-road machinery) of the EMEP EMEP/EEA air pollutant emission inventory guidebook 2019 (EMEP/EEA, 2019a, b). This source category includes exhaust emissions related to fuel consumption of off-road vehicles and other machinery used in agriculture. On-site activity data on fuel consumption were derived from farmers' questionnaires.
- Tier 1 methodology was used for calculating N₂O emissions from fertilizer application in agricultural soils, according to the default value of 1% of kg⁻¹ fertilizer N applied of IPCC (IPCC, 2006).
- Tier 2 methodology was applied for the calculation of NH₃ emissions resulting from soil fertilization, taking into account the climate zone of the pilot farm, the soil pH, and the amount of N applied to the soil as calculated from the information in the farmers' questionnaires and logbooks. The EFs were selected based on the fertilizer type as recorded by the farmer and applied on each pilot farm, according to Table 3.2 EFs for NH₃ emissions from fertilizers (in g NH₃ (kg N applied)⁻¹) from the EMEP EMEP/EEA air pollutant emission inventory guidebook 2019 (EMEP/EEA, 2019a, b).

The tier 1 EFs used to calculate the emissions for all atmospheric pollutants emitted from agricultural activities, apart from fertilizer related NH₃, are summarized in Table 3. Tier 2 EFs for NH₃ calculation are related to the fertilizer type applied and can be found in Table 3.2 of the EMEP/EEA air pollutant emission inventory guidebook 2019 (EMEP/EEA, 2019a, b).

In addition to the above calculations of emissions, a sensitivity analysis on the effect of temporal variation of emissions on air pollutant local concentrations was performed for the Ellassona 6 field, for which emissions were calculated per day, on the basis of the recorded fertilizer application dates within the baseline and the SF application year. In particular, 8 application days were recorded for 2019 and 6 for 2020. The emissions were considered to be 0 for the rest of the days.

Table 3 Emission factors (EFs) from NFR categories

| Pollutants | NFR category | | | |
|-------------------|---|------------------------------------|--|---|
| | Fertilizer application (NFR 3D) | Non-road machinery (NFR 1.A.4 cii) | Standing crops (NFR 3D) (kg ha ⁻¹) | Agricultural operations (NFR 3D) (kg ha ⁻¹) |
| PM ₁₀ | – | 1913 g·tonnes ⁻¹ fuel | – | 1.56 |
| PM _{2.5} | – | 1913 g·tonnes ⁻¹ fuel | – | 0.06 |
| NO _x | – | 34,457 g·tonnes ⁻¹ fuel | – | – |
| NO | 0.04 kg NO ₂ kg ⁻¹ fertilizer N applied | – | – | – |
| NMVOC | – | 3542 g·tonnes ⁻¹ fuel | 0.86 | – |
| NH ₃ | Table 3.2 ^a | 8 g·tonnes ⁻¹ fuel | – | – |
| N ₂ O | 0.01 kg N ₂ O–N (kg N) ^{-1b} | 136 g·tonnes ⁻¹ fuel | – | – |
| CO ₂ | – | 3160 kg·tonnes ⁻¹ fuel | – | – |
| CH ₄ | – | 87 g·tonnes ⁻¹ fuel | – | – |

All EFs (except the EF of N₂O from fertilizer application) are based on EMEP/EEA air pollutant emission inventory guidebook 2019.

All EFs are tier 1, except the ones of NH₃ from fertilizer application which are tier 2.

^aSee Table 3.2 in EMEP/EEA air pollutant emission inventory guidebook 2019.

^bEF of N₂O from fertilizer application is based on 2006 IPCC Guidelines for National Greenhouse Gas Inventories.

Methodology for dispersion simulations

The contribution of emitted pollutants on ambient concentrations and deposition rates around the pilot fields was assessed by performing dispersion calculations for a period of a year. For this assessment, three pilot fields were chosen on the basis of the completeness of activity and emission information and the availability of local meteorological measurements. These are the Ellassona 6, Mirabello 2, and Pella 3 fields, located in Central, Southern, and Northern parts of Greece, respectively, and in this way representing different climatic and meteorological regimes of a Mediterranean region. The Lagrangian dispersion model AUSTAL2000 (Janicke 2002; Janicke et al. 2003) was applied on computational domains with a total extent of $5 \times 5 \text{ km}^2$ around each pilot field, and a grid resolution of 20 m.

For the assessment of dispersion in the surrounding areas, yearly average fields of concentration increments for the pollutants NO_x , PM_{10} , NH_3 , VOCs, and N_2O were calculated, as well as deposition fields for PM_{10} and NH_3 . In addition to yearly averages, additional concentration percentiles and maximum values were calculated for the reference period in line with the limit values and averaging periods specified by the EU directive for the protection of human health (2008/50/EC). These values were calculated as concentration increments due to the farming emissions, on a set of representative virtual receptor sites lying inside, near and further away from each pilot field. Given that the particular model operates under a linear assumption for concentrations, calculated concentrations represent increments attributed to the emissions under consideration. Oxidation rates of NO in AUSTAL2000 depend only on temperature and atmospheric stability class, therefore background concentrations could be set to zero for all pollutants without affecting the calculated concentration and deposition increments.

Driving meteorology was obtained from hourly time series of on-site meteorological observations of wind speed, direction and temperature for the year 2020, while the atmospheric stability hourly state was determined using the Turner's method (Turner, 1970) using cloud cover information from the nearest airport. The aerodynamic roughness length was calculated using land use maps for the application areas and was set to $z_0 = 0.1 \text{ m}$ for all three pilot fields. The effects of local topography were taken into account by incorporating information from Digital Elevation Maps with a resolution of 90 m and the use of the diagnostic field flow model TALdia. For both the baseline and application periods, a common meteorological input was used, corresponding to the 2020 conditions.

Emissions from all activities were represented as polygonal area sources coinciding with the limits of each pilot field. Activities realistically occurring outside the field, i.e., transport of on-road machinery or material spillage were

also incorporated in the polygonal area. The nominal emission height for both exhaust and suspension sources was set to 2 m above ground. As usual in the application of AUSTAL2000 over long periods, emission rates were considered constant throughout the simulation period, with the exception of NH_3 emissions in the Ellassona case, which were introduced as a time-variable series depending on the dates of fertilizer application. The fact that agricultural activities occur under a variety of meteorological and atmospheric stability conditions throughout the cultivation period minimizes any bias that is introduced by this assumption.

Results

Results of emissions calculation

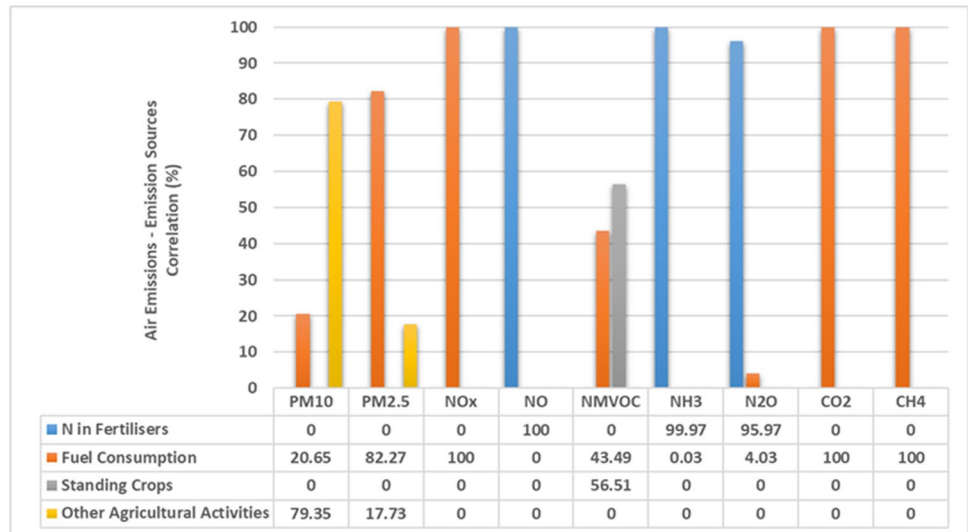
The results of emissions calculation indicate the correlation of the studied pollutants to major contributing emissions sources in agriculture. The contribution % of each agricultural source to the total emissions of the studied pollutants was calculated and the results are presented in Fig. 3. The relevant contributions result due to the EFs attributed to each source type in the combined tier 1/tier 2 emissions calculation methodology used in the present paper, as described in the in EMEP/EEA air pollutant emission inventory guidebook 2019. The contribution ratios of Fig. 3 were calculated by applying the following equation to each air pollutant and GHG individually:

$$[\text{Emissions from each source (g)} / \text{Total emissions from all sources (g)}] \cdot 100.$$

Emission results only from the crop fields for which fuel consumption data were available (Ellassona 6, Pella 3, 4, & 5, Mirabello 2 & 4, Stylida 4) were used, for the year 2019 and/or 2020 (see Table 2). The final percentage values were calculated from the average values of these pilot areas and cultivation years.

From the analysis it is shown that, according to the emissions calculation methodology used in the present paper, emissions for NO_x , CO_2 , and CH_4 result entirely from fuel combustion in non-road machinery, while N fertilizer application contributes to NO emissions by 100%. NH_3 and N_2O are also almost exclusively emitted from N fertilizer application, by 99.97% and 95.97% respectively, while a small percentage (0.03% and 4.03% respectively) is emitted from fuel consumption activities. Agricultural activities (other agricultural activities such as ploughing, spraying, harvesting, and storage/handling of agricultural products) are responsible for 79.35% of PM_{10} emissions and for 17.73% of $\text{PM}_{2.5}$ emissions, whereas fuel consumption of non-road machinery contributes by 20.65% to PM_{10} emissions and by 82.27% to $\text{PM}_{2.5}$ emissions. Standing crop emissions are the main source of NMVOCs, contributing by 56.6% to total

Fig. 3 Contribution (%) of major agricultural emissions sources to air pollutants and GHGs emissions



emissions, while a smaller but significant contribution to NMVOCs agricultural emissions is related to fuel consumption (43.49%).

As demonstrated in Fig. 4 and based on the statistical analysis performed, particulate matter and NMVOC pollutants in the pilot fields are emitted mainly as a result of fuel consumption. The highest total emissions of all three pollutants are calculated in the case of Styliida, where also the highest fuel consumption data (562 lt/ha for 2019 and 524 lt/ha for 2020) are reported by farmers. In all pilot cases, emissions of PM and NMVOCs follow the trendline of the amount of fuel consumed in agricultural activities. The decrease noted in emissions of all relevant pollutants in Mirabello and Pella in 2020 compared to 2019 is related to the reduction in fuel consumed by farmers in 2020, as a result of conforming to the SF advice. In Ellassona, fuel

consumption remained the same for the 2 years studied, resulting in unchanged pollutant emissions.

Figure 5 presents the correlation between the total emissions (in g/ha) of NH₃ and N₂O and NO, and the amount of fertilizer applied. Kiwi is the crop with the highest amount of N fertilizer applied in both studied years (247 and 166 kg/ha respectively) and the highest emissions (23,179 g/ha of NH₃, 2468 g/ha of N₂O, and 9870 g/ha of NO in 2019 and 12,033 g/ha of NH₃, 1664 g/ha of N₂O, and 6654 g/ha of NO in 2020), while the lowest amount of N fertilizer is applied in the case of olive production (Styliida) in 2019 (56.1 kg/ha) and walnut production (Ellassona) in 2020 (47 kg/ha). In the case of Ellassona, the low N fertilizer results to the lowest related emissions (6177 g/ha of NH₃, 701 g/ha of N₂O, and 2654.8 g/ha of NO in 2019 and 4225 g/ha of NH₃, 502 g/ha of N₂O, and 1860 g/ha of NO in 2020) between the different

Fig. 4 Calculated emissions of PM₁₀, PM_{2.5}, and NMVOCs in the studied pilot areas, in relation to fuel consumption in 2019 and 2020

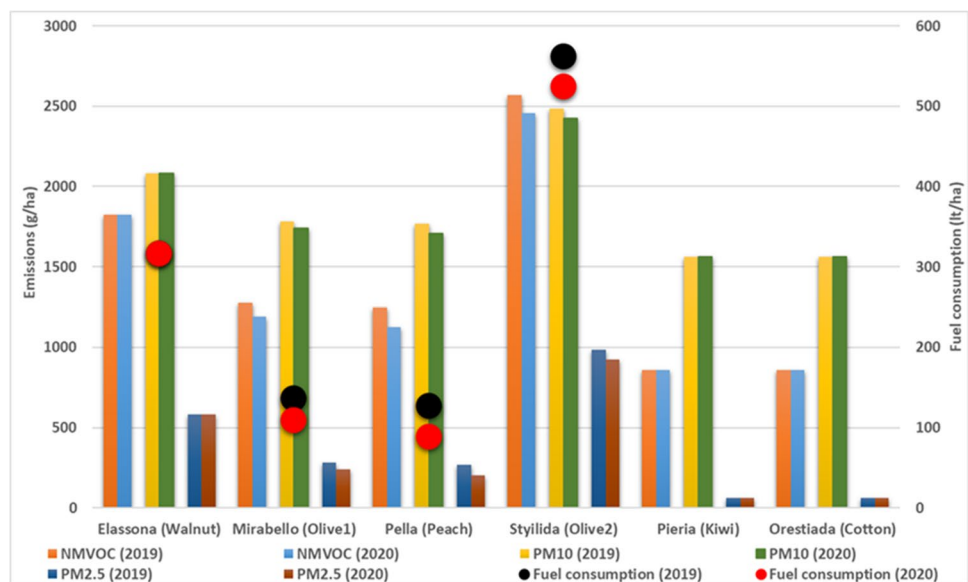
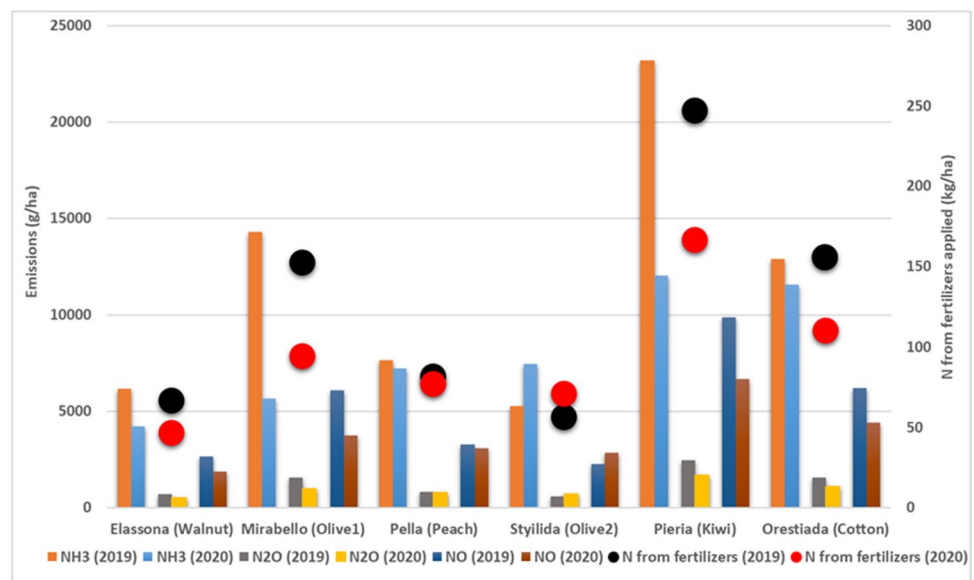


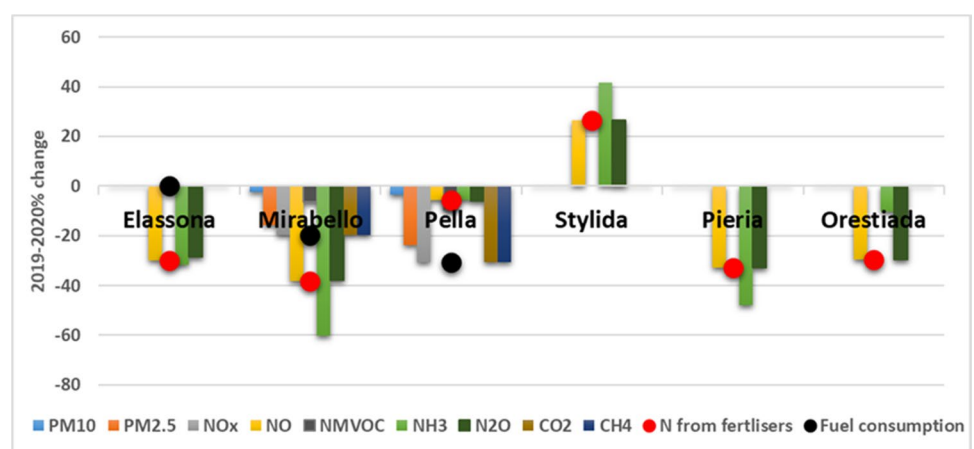
Fig. 5 Calculated emissions of NH_3 , N_2O , and NO in the studied pilot areas, in relation to N fertilizer applied in 2019 and 2020



pilot areas. In all pilot fields, apart from Stylida, SF application resulted in reduced N fertilizer quantities applied, leading to lower emissions of the relevant pollutants.

The regional intercrop variations in NH_3 emissions are related not only to the difference in the amount of N in the fertilizers applied, but also to the different EF allocated to the specific fertilizer type used. The tier 2 EFs used for the calculation of NH_3 emissions vary considerably according to the fertilizer type. For example, NPK mixtures, such as the ones applied in the case of olive crops, have high EFs of 94 g NH_3 per kg of N in fertilizers for temperate climate and high pH, whereas for the same climatic and soil conditions, the EF of AN mixtures, such as those used in the case of cotton, is only 33 g NH_3 per kg of N in fertilizers. In this case, Fig. 5 shows that, despite of the fact that the amount of N in fertilizers in Orestiada (155 kg/ha), is slightly bigger than in Mirabello (152 kg/ha) in 2019, NH_3 emissions are significantly lower (12,886 g/ha in Orestiada compared to 14,289 g/ha in Mirabello).

Fig. 6 Percentage % change of emissions in relation to percentage change in fuel consumption and the amount of nitrogen (N) in the fertilizers applied between 2019 and 2020



For the evaluation of the efficiency of the SF application in terms of reduction of atmospheric emissions, the differences in emissions of all pollutants for all pilot sites between the baseline year 2019 and the first SF application year 2020 were calculated (Fig. 6). In the majority of the participating pilot fields, SF resulted in reduction of air pollutants and GHG emissions due to the lower amount of fuel consumed and N fertilizer applied. In four out of the six studied pilot areas, the quantity of N fertilizer applied was reduced by around 30%, reaching a significant 38.16% decrease in the case of Mirabello (olive crop), a 32.58% decrease in Pieria (kiwi), 29.94% in Ellassona (walnut), and 29.32% in Orestiada (cotton). In these pilot areas, an equal decrease in NO emissions was estimated, as in the methodology used in the present paper, NO is emitted entirely from N fertilizer application. As described in detail in the previous paragraphs, pollutant emissions mainly attributed to N fertilizer application include also NH_3 and N_2O , which

are also reduced in 2020 by up to 60.4% for NH_3 and by up to 37.97% for N_2O , both in Mirabello pilot area (olive crop). Mirabello pilot area demonstrates the largest NH_3 emission reduction compared to other areas, which could be attributed to the SF advice to change the fertilizer type in addition to lower fertilizer quantity. AN fertilizer was applied in 2020 in Mirabello 4 field, which has a significantly lower EF compared to NPK applied in the baseline year, as described in detail in the previous paragraph. A small reduction of 5.74% in fuel consumption in Pella pilot area was reported by farmers, leading to less significant decrease in the emissions of the related pollutants. Stylida is the only pilot area in which N fertilizer applied has increased in 2020 (by 26.4%), resulting to substantial increases in emissions of NH_3 (by 41.58%), NO , and N_2O (both increased by 26.4% as fuel consumption data were not available for Stylida and relevant emissions resulted solely from fertilizer application). The increase in fertilizer application may be attributed to the fact that the farmers in the specific area were not willing to follow the SF advice in 2020.

Fuel consumption data were available only for three out of the six participating pilot areas, namely Ellassona, Mirabello, and Pella. As shown in Fig. 6, fuel consumption in Ellassona remained unchanged between 2019 and 2020, thus no differences were calculated in the emissions of relevant pollutants (NO_x , NMVOC, PM, and GHGs: CO_2 and CH_4).

A substantial decrease in fuel consumption in 2020 compared to 2019 was reported by farmers in Mirabello (by 19.8%) and in Pella (by 30.56%), resulting to equal reductions in emissions of NO_x , CO_2 , and CH_4 as the only contributing source for these pollutants are fuel consumption activities, and to significant reductions in $\text{PM}_{2.5}$ emissions (by 15.61% in Mirabello and 23.74% in Pella).

Air pollutant dispersion results

Three sets of receptor points were defined to assess the pollution effect due to emissions within each field. The locations of these points in the corresponding computational domains for the three selected pilot fields are shown in Fig. 7.

Annual average concentration increments of NO_x , calculated for the Ellassona 6 pilot field, are shown in Fig. 8 (left). The spatial maximum corresponds to a value less than $1 \mu\text{g}/\text{m}^3$ and is located within the limits of the emission polygon. As evident by the plume shape, the prevailing wind is causing a preferential dispersion toward the south-SE direction with the concentration increment rapidly decreasing by an order of magnitude within the first 1 km from the source. A slight topography-induced effect is also visible due to the presence of hill on the western part of the domain. Due to the lack of any non-linear chemistry in the model, the average plumes of other pollutants follow a similar distribution.

Deposition fields for PM_{10} follow a very similar spatial distribution, as shown in Fig. 8 (middle). On the other hand, NH_3 deposition (Fig. 8, right) has pronounced lobes corresponding to the time-dependent emissions from the application of fertilizer during specific periods of the year. PM_{10} deposition rates have a maximum of around $6 \cdot 10^{-5} \text{ g}/(\text{m}^2 \text{ day})$, while NH_3 deposition rates lie below $0.56 \text{ kg}/\text{ha}/\text{year}$. For both pollutants, the bulk of the total deposition occurs within the limits of the field.

Table 4 summarizes the quantification of the pollution burden under the baseline (2019) and 2020 periods for the three most representative receptor points and for the average domain. It is evident that for NO_2 and ammonia both the concentration and deposition increments undergo a decrease directly consistent with the corresponding reduction in emissions. Ammonia concentrations and deposition depend on the days of fertilizer application which were different

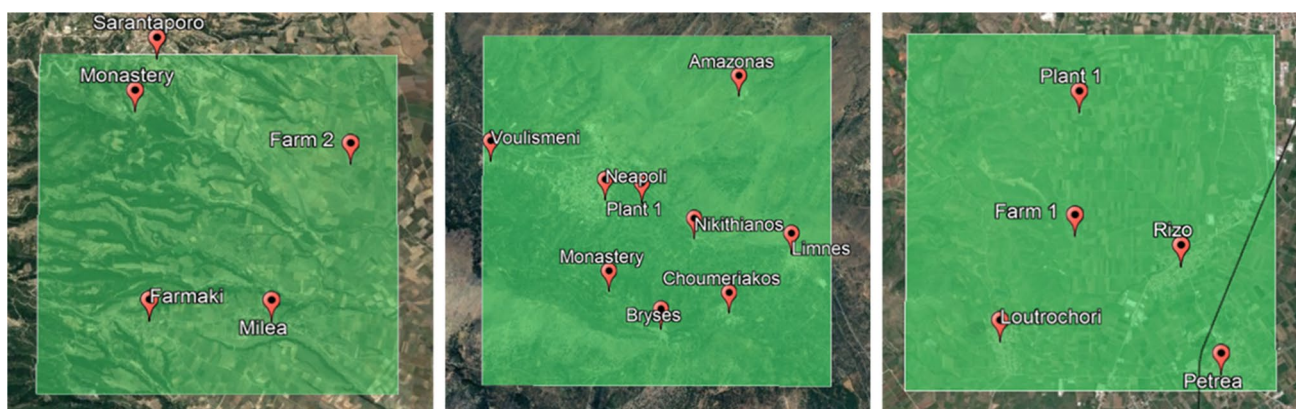


Fig. 7 AUSTAL2000 computational domains and receptor points for Ellassona 6 (left), Mirabello 2 (middle), and Pella 3 (right) pilot fields

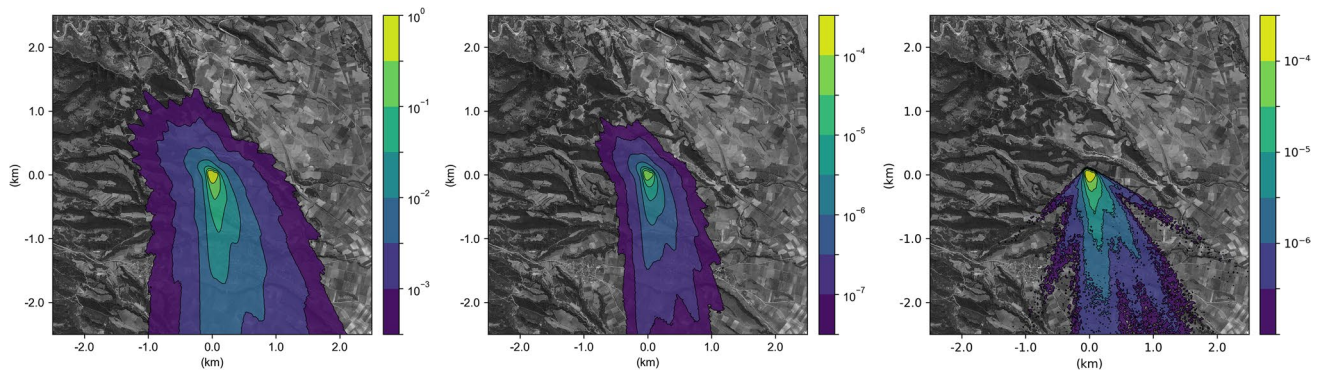


Fig. 8 Annual average fields of NO_x surface concentration increment, in μg/m³ (left), and deposition rate increments of PM₁₀ (middle) and NH₃(right), in g/(m² day), calculated around the Ellassona 6 pilot field for 2019

Table 4 Reductions of annual average concentrations and deposition rates in three representative receptor points of the Ellassona 6 pilot field and for the average domain

| Location | Field_SW | | Mhlia | | Monastery | | Domain average | |
|------------------|-------------------------------------|---------------------------------|-------------------------------------|---------------------------------|-------------------------------------|---------------------------------|-------------------------------------|---------------------------------|
| | Average annual reduction | Annual percentage reduction (%) | Average annual reduction | Annual percentage reduction (%) | Average annual reduction | Annual percentage reduction (%) | Average annual reduction | Annual percentage reduction (%) |
| Pollutant | Concentrations (μg/m ³) | Concentrations | Concentrations (μg/m ³) | Concentrations | Concentrations (μg/m ³) | Concentrations | Concentrations (μg/m ³) | Concentrations |
| NO ₂ | 1.74·10 ⁻³ | 29.95 | 9.79·10 ⁻⁵ | 29.93 | 5.87·10 ⁻⁶ | 29.93 | 3.57·10 ⁻⁵ | 29.94 |
| NO _x | 0 | 0 | 0 | 0 | 0 | 0 | 0 | 0 |
| VOC | 0 | 0 | 0 | 0 | 0 | 0 | 0 | 0 |
| PM ₁₀ | 0 | 0 | 0 | 0 | 0 | 0 | 0 | 0 |
| NH ₃ | 1.37·10 ⁻² | 4.88 | 1.05·10 ⁻³ | 98.44 | 6.45·10 ⁻⁸ | 19.19 | 9.18·10 ⁻⁵ | 13.57 |
| | Deposition g/(m ² day) | Deposition | Deposition g/(m ² day) | Deposition | Deposition g/(m ² day) | Deposition | Deposition g/(m ² day) | Deposition |
| PM ₁₀ | 0 | 0 | 0 | 0 | 0 | 0 | 0 | 0 |
| | Deposition g/(m ² day) | Deposition | Deposition g/(m ² day) | Deposition | Deposition g/(m ² day) | Deposition | Deposition g/(m ² day) | Deposition |
| NH ₃ | 1.53·10 ⁻⁵ | 8.76 | 9.18·10 ⁻⁷ | 99 | 4.4·10 ⁻¹⁰ | 100 | 7.83·10 ⁻⁸ | 18.76 |

between 2019 and 2020; therefore, the corresponding reductions at the receptor points are not directly comparable. For the rest of the pollutants, no decrease is noted in line with the assumption of constant corresponding emissions. It should be further noted that the apparent discrepancy between the behavior of NO₂ and NO_x in this set of simulations is due to the independent treatment as separately-emitted pollutants, where the bulk of dispersed NO₂ is assumed to be produced by oxidation of primary emitted NO.

In Fig. 9 (left), annual average concentration increments of NO_x for the Mirabello 2 pilot field are shown. The spatial maximum corresponds to less than 0.1 μg/m³ and is located near the southern boundary of the emission polygon. The plume has two prominent lobes to the N-NW to S-SE direction, while the same order-of-magnitude decrease within the first 1 km from the source is observed for NO_x as in the

Ellassona case. Deposition fields for PM₁₀ and NH₃ follow a very similar spatial distribution, as shown in Fig. 9 (middle, right). PM₁₀ deposition rates have a maximum of around 1·10⁻⁵ g/(m² day), while NH₃ deposition rates lie below 1.35·10⁻⁴ g/(m² day). For both pollutants, the bulk of the total deposition occurs within the limits of the field.

Table 5 summarizes the pollution burden under the baseline (2019) and 2020 periods for the selected receptor points. As in the Ellassona 6 case, the concentration increments of gaseous pollutants are decreasing almost linearly with the corresponding reduction in emissions. In the case of PM₁₀, the near-field concentrations are dominated by the smaller reduction of the coarse PM component, while in larger distances, the reduction of the PM_{2.5} component becomes more significant. The decrement of PM₁₀ deposition rates for 2020 is dominated by the small reduction in

the coarse component emission, while deposition rates for NH_3 decrease linearly with the corresponding emissions.

Figure 10 (left) shows the annual average concentration increments of NO_x for the Pella 3 pilot field. The spatial

maximum corresponds to less than $0.2 \mu\text{g}/\text{m}^3$ and is located near the northern boundary of the emission polygon. The average plume is dispersed toward the south, with an apparent distortion caused by the local topography in the western

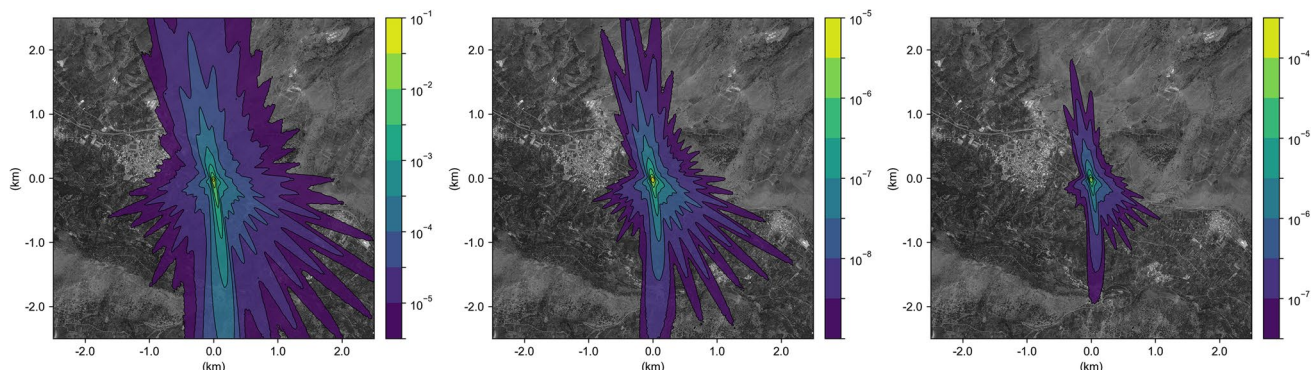


Fig. 9 Annual average fields of NO_x surface concentration increment, in $\mu\text{g}/\text{m}^3$ (left), and deposition rate increments of PM_{10} (middle) and NH_3 (right), in $\text{g}/(\text{m}^2\text{d})$, calculated around the Mirabello 2 pilot field for 2019

Table 5 Reductions of annual average concentrations and deposition rates in three representative receptor points of the Mirabello 2 pilot field

| Location | Field_SW | | Bryses | | Limnes | |
|------------------|--|---------------------------------|--|---------------------------------|--|---------------------------------|
| | Average annual reduction | Annual percentage reduction (%) | Average annual reduction | Annual percentage reduction (%) | Average annual reduction | Annual percentage reduction (%) |
| Pollutant | Concentrations ($\mu\text{g}/\text{m}^3$) | Concentrations | Concentrations ($\mu\text{g}/\text{m}^3$) | Concentrations | Concentrations ($\mu\text{g}/\text{m}^3$) | Concentrations |
| NO_2 | $4.03 \cdot 10^{-5}$ | 41.66 | $5.1 \cdot 10^{-5}$ | 41.64 | $5.58 \cdot 10^{-7}$ | 41.66 |
| NO_x | $4.31 \cdot 10^{-3}$ | 40 | $1.3 \cdot 10^{-4}$ | 40 | $2.39 \cdot 10^{-6}$ | 40 |
| VOC | $4.43 \cdot 10^{-4}$ | 17.61 | $1.34 \cdot 10^{-5}$ | 17.6 | $2.45 \cdot 10^{-7}$ | 17.56 |
| PM_{10} | $2.35 \cdot 10^{-4}$ | 8.25 | $5.18 \cdot 10^{-6}$ | 15.86 | $1.08 \cdot 10^{-7}$ | 12.79 |
| NH_3 | $8.15 \cdot 10^{-3}$ | 41.69 | $6.62 \cdot 10^{-5}$ | 41.68 | $1.99 \cdot 10^{-6}$ | 41.67 |
| PM_{10} | Deposition $\text{g}/(\text{m}^2 \text{ day})$ | Deposition | Deposition $\text{g}/(\text{m}^2 \text{ day})$ | Deposition | Deposition $\text{g}/(\text{m}^2 \text{ day})$ | Deposition |
| | $1.9 \cdot 10^{-8}$ | 1.26 | $4.01 \cdot 10^{-10}$ | 4.39 | $9 \cdot 10^{-12}$ | 2.19 |
| NH_3 | Deposition $\text{g}/(\text{m}^2 \text{ day})$ | Deposition | Deposition $\text{g}/(\text{m}^2 \text{ day})$ | Deposition | Deposition $\text{g}/(\text{m}^2 \text{ day})$ | Deposition |
| | $5.4 \cdot 10^{-6}$ | 41.67 | $2.97 \cdot 10^{-8}$ | 41.67 | $1.43 \cdot 10^{-9}$ | 41.68 |

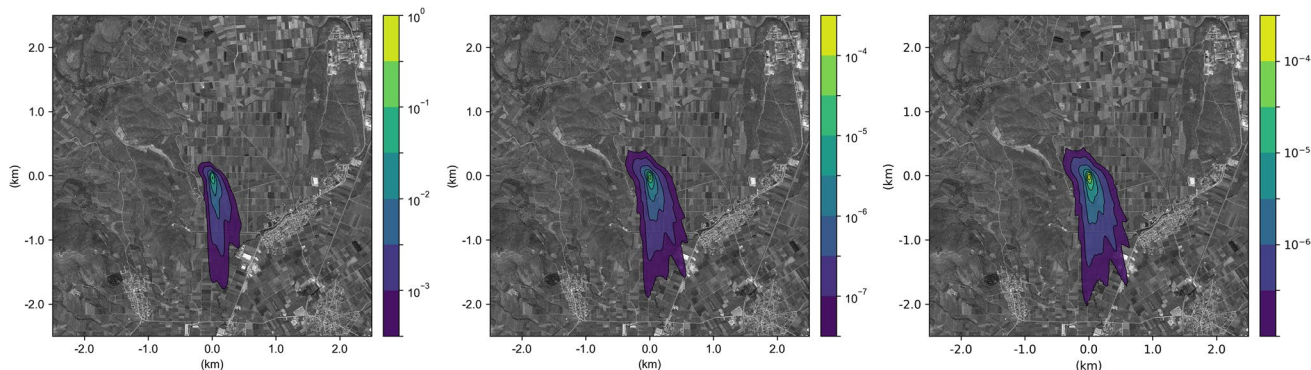


Fig. 10 Annual average fields of NO_x surface concentration increment, in $\mu\text{g}/\text{m}^3$ (left), and deposition rate increments of PM_{10} (middle) and NH_3 (right), in $\text{g}/(\text{m}^2 \text{ day})$, calculated around the Pella 3 pilot field for 2019

Table 6 Reductions of annual average concentrations and deposition rates in three representative receptor points of the Pella 3 pilot field

| Location | Field_SW | | Rizo | | Petrea | |
|------------------|---|---------------------------------|---|---------------------------------|---|---------------------------------|
| | Average annual reduction | Annual percentage reduction (%) | Average annual reduction | Annual percentage reduction (%) | Average annual reduction | Annual percentage reduction (%) |
| Pollutant | Concentrations ($\mu\text{g}/\text{m}^3$) | Concentrations | Concentrations ($\mu\text{g}/\text{m}^3$) | Concentrations | Concentrations ($\mu\text{g}/\text{m}^3$) | Concentrations |
| NO ₂ | 0 | 0 | 0 | 0 | 0 | 0 |
| NO _x | $6.9 \cdot 10^{-3}$ | 37.52 | $2.33 \cdot 10^{-5}$ | 37.5 | $2.28 \cdot 10^{-5}$ | 37.51 |
| VOC | $7.09 \cdot 10^{-4}$ | 9.81 | $2.39 \cdot 10^{-6}$ | 9.79 | $2.35 \cdot 10^{-6}$ | 9.84 |
| PM ₁₀ | $3.63 \cdot 10^{-4}$ | 4.52 | $9.9 \cdot 10^{-7}$ | 7.47 | $8.93 \cdot 10^{-7}$ | 8.59 |
| NH ₃ | 0 | 0 | 0 | 0 | $1 \cdot 10^{-8}$ | 0.04 |
| | Deposition g/(m ² day) | Deposition | Deposition g/(m ² day) | Deposition | Deposition g/(m ² day) | Deposition |
| PM ₁₀ | $3.3 \cdot 10^{-8}$ | 0.69 | $7.8 \cdot 10^{-11}$ | 1.23 | $7.6 \cdot 10^{-11}$ | 1.47 |
| | Deposition g/(m ² day) | Deposition | Deposition g/(m ² day) | Deposition | Deposition g/(m ² day) | Deposition |
| NH ₃ | $2.7 \cdot 10^{-9}$ | 0.02 | $2.7 \cdot 10^{-12}$ | 0.01 | $2.7 \cdot 10^{-12}$ | 0.01 |

part of the domain. Concentrations decrease almost by two orders of magnitude within the first 1 km from the source. Deposition fields for PM₁₀ and NH₃ follow a very similar spatial distribution, as shown in Fig. 10 (middle, right). PM₁₀ deposition rates have a maximum of around $5 \cdot 10^{-5}$ g/(m² day) while NH₃ deposition rates lie below $1.62 \cdot 10^{-4}$ g/(m² day). For both pollutants, the bulk of the total deposition occurs within a distance 100 m from the field.

Table 6 summarizes the pollution burden under the baseline (2019) and 2020 periods for the selected receptor points. As in the Mirabello 2 case, the concentration increments are decreasing almost linearly with the corresponding reduction in emissions for NO_x and VOC and are almost constant for the rest of the pollutants, in line with the negligible reduction in their emissions rates. PM₁₀ reductions are dominated by the (smaller) reduction of the coarse fraction near the field and increase toward the larger reduction of the PM_{2.5} component as we move further away. The decrement of PM₁₀ deposition rates for 2020 is dominated by the small reduction in the coarse component emission, while deposition rates for NH₃ decrease linearly with the corresponding emissions.

Conclusions

SF application emerges as an efficient and robust tool for implementing the EU policies in the areas of water, waste and air management, by reducing the contribution of the agricultural sector over the major environmental burdens. Atmospheric modeling is one of several components contributing to the comprehensive evaluation of the environmental impact of SF application. In the present paper, a Lagrangian dispersion model was used for atmospheric simulations to assess the efficiency of the SF

GAIA Sense system in terms of local air quality improvement, which relies in a large degree on realistic atmospheric emissions data. The methodology for calculating emissions of atmospheric pollutants and GHGs related to the agricultural activities of the participating pilot farms was based on a combined tier 1 and tier 2 approach from the EMEP/EEA and IPCC guidebooks and on farm-level activity information from farmers' replies to targeted questionnaires, in the frame of the LIFE GAIA Sense project. The results of the present study indicate the potential benefits of SF application in the studied pilot areas in terms of improvement of local air quality, for most pollutants in direct proportion to the reduction in the corresponding emission rates. Reduction in PM deposition is dependent on the mix of coarse–fine fractions, but generally follows a clearly decreasing trend. Taking into account the effect of temporal variation in emissions, in order to account for individual days of fertilizer application, causes a change in the spatial distribution of deposited and dispersed mass but without noticeable change in the calculated spatial average and maxima. The noted emission reductions percentages achieved could not be generalized for other crops or application areas, as the SF advice is adapted to the particular crop field on the basis of selected geospatial, soil, meteorological, and crop information. Further studies on additional participating fields are necessary to support the encouraging results of the present study on the beneficial impact of SF on local air quality in agricultural areas.

Acknowledgements The “LIFE GAIA Sense” Project is co-funded by the LIFE Programme of the European Union under contract number LIFE17 ENV/GR000220.

Funding Open access funding provided by HEAL-Link Greece This work was supported by the “LIFE GAIA Sense” Project, which is co-funded by the LIFE Programme of the European Union under contract number LIFE17 ENV/GR000220.

Data availability The datasets generated during and/or analyzed during the current study are not publicly available as they were acquired from personal questionnaires to farmers but are available from the corresponding author on reasonable request. On-site meteorological measurements were obtained from GAIATrons stations installed and operated by Neupublic S.A.

Declarations

Competing interests The authors declare no competing interests.

Ethics approval and consent to participate Not applicable.

Consent for publication Not applicable.

Open Access This article is licensed under a Creative Commons Attribution 4.0 International License, which permits use, sharing, adaptation, distribution and reproduction in any medium or format, as long as you give appropriate credit to the original author(s) and the source, provide a link to the Creative Commons licence, and indicate if changes were made. The images or other third party material in this article are included in the article's Creative Commons licence, unless indicated otherwise in a credit line to the material. If material is not included in the article's Creative Commons licence and your intended use is not permitted by statutory regulation or exceeds the permitted use, you will need to obtain permission directly from the copyright holder. To view a copy of this licence, visit <http://creativecommons.org/licenses/by/4.0/>.

References

- Almaraz M, Bai E, Wang C, Trousdell J, Conley S, Faloona I, Houlton BZ (2018) Agriculture is a major source of NO_x pollution in California. *Science Advances* 4(6). <https://doi.org/10.1126/sciadv.aau2561>
- Dennis RL, Mathur R, Pleim JE, Walker JT (2010) Fate of ammonia emissions at the local to regional scale as simulated by the Community Multiscale Air Quality model. *Atmos Pollut Res* 1(4):207–214. <https://doi.org/10.5094/APR.2010.027>
- EEA (2019a) European Union emission inventory report 1990–2017 under the UNECE Convention on Long-range Transboundary Air Pollution (LRTAP). European Environmental Agency. <https://www.eea.europa.eu/Posted22> July 2019a
- EEA (2019b) Annual European Union greenhouse gas inventory 1990–2017 and inventory report 2019b European Environmental Agency. <https://www.eea.europa.eu> Published 29 May 2019
- EMEP/EEA (2019) EMEP/EEA air pollutant emission inventory guidebook 2019 Technical guidance to prepare national emission inventories. European Environmental Agency. <https://www.eea.europa.eu/Posted> 17 October 2019
- Erismann JW, Schaap M (2004) The need for ammonia abatement with respect to secondary PM reductions in Europe. *Environ Pollut* 129(1):159–163. <https://doi.org/10.1016/j.envpol.2003.08.042>
- Gu Y, Wong TW, Law SC, Dong GH, Ho KF, Yang Y and Yim SHL (2018) Impacts of sectoral emissions in China and the implications: air quality, public health, crop production, and economic costs. *Environ Res Lett* 13(8). <https://doi.org/10.1088/1748-9326/aad138>
- Gyldenkaerne S, Skjøth CA, Hertel O, Ellermann T (2005) A dynamical ammonia emission parameterization for use in air pollution models. *J Geophys Res* 110(7):D07108. <https://doi.org/10.1029/2004JD005459>
- IPCC (2006) IPCC Guidelines for National Greenhouse Gas Inventories, 4(11). Intergovernmental Panel on Climate Change. <https://www.ipcc-nggip.iges.or.jp>. Published 2019
- Janicke L. and U. Janicke (2003) (A modelling system for licensing industrial facilities) Entwicklung eines modellgestützten Beurteilungs Systems für den anlagenbezogenen Immissionschutz. UFOPLAN 200 43 256, on behalf of the German Federal Environmental Agency (UBA)
- Janicke L. (2002) Lagrangian dispersion modelling. Particulate Matter in and from Agriculture, 235, 37–41, ISBN 3–933140–58–7
- Lieder S. and C. Schröter-Schlaack (2021) Smart farming technologies in arable farming: towards a holistic assessment of opportunities and risks. *Sustainability* 13 (12). <https://doi.org/10.3390/su13126783>
- Park S-K, Cobb CE, Wade K, Mulholland J, Yongtao Hu, Russell AG (2006) Uncertainty in air quality model evaluation for particulate matter due to spatial variations in pollutant concentrations. *Atmos Environ* 40:563–573. <https://doi.org/10.1016/j.atmosenv.2005.11.078>
- Pozzer A, Tsimpidi AP, Karydis VA, de Meij A, Lelieveld J (2017) Impact of agricultural emission reductions on fine-particulate matter and public health. *Atmospheric Chem Physics* 17:12813–12826. <https://doi.org/10.5194/acp-17-12813-2017>
- Theobald MR, Løfstrøm P, Walker J, Andersen HV, Pedersen P, Vallejo A, Sutton MA (2012) An intercomparison of models used to simulate the short-range atmospheric dispersion of agricultural ammonia emissions. *Environ Model Softw* 37:90–102. <https://doi.org/10.1016/j.envsoft.2012.03.005>
- Turner DB (1970) Workbook of atmospheric dispersion estimates, Office of Air Program Pub. No. AP-26. Environmental Protection Agency, USA
(N.D) URL1:<https://lifegaiasense.eu>
- Zhang Y, Shiang-Yuh W, Krishnan S, Wang K, Queen A, Aneja VP, Pal Arya S (2008) Modeling agricultural air quality Current status, major challenges, and outlook. *Atmos Environ* 42(14):3218–3237
- Zhao ZO, Bai ZH, Winiwarer W, Kiesewetter G, Heyes C, Ma L (2017) Mitigating ammonia emission from agriculture reduces PM_{2.5} pollution in the Hai River Basin in China. *Sci Total Environ* 609:1152–1160. <https://doi.org/10.1016/j.scitotenv.2017.07.240>

Publisher's note Springer Nature remains neutral with regard to jurisdictional claims in published maps and institutional affiliations.